AZD4625 is a Potent and Selective Inhibitor of KRAS^{G12C}

Atanu Chakraborty[1], Lyndsey Hanson[1], David Robinson[1], Hilary Lewis[1], Sue Bickerton[1], Michael Davies[1], Radoslaw Polanski[1], Rebecca Whiteley[1], Alex Koers[1], James Atkinson[1], Tamara Baker[1], Ivan del Barco Barrantes[1], Giovanni Ciotta[1], Jason G. Kettle[1], Lukasz Magiera[1], Carla P. Martins[1], Alison Peter[1], Eleanor Wigmore[1], Zoe Underwood[1], Sabina Cosulich[1], Michael Niedbala[2], and Sarah Ross[1]

ABSTRACT

AZD4625 is a potent, selective, and orally bioavailable inhibitor of oncogenic KRAS^{G12C} as demonstrated in cellular assays and *in vivo* in preclinical cell line–derived and patient-derived xenograft models. *In vitro* and cellular assays have shown selective binding and inhibition of the KRAS^{G12C} mutant isoform, which carries a glycine to cysteine mutation at residue 12, with no binding and inhibition of wild-type RAS or isoforms carrying non-KRAS^{G12C} mutations. The pharmacology of AZD4625 shows that it has the potential to provide therapeutic benefit to patients with *KRAS*^{G12C} mutant cancer as either a monotherapy treatment or in combination with other targeted drug agents.

Introduction

KRAS is commonly mutated in human cancer with activating alterations reported in 9% to 15% of tumors (1, 2). The prevalence of *KRAS* mutations differs upon tumor type and they are particularly enriched in pancreatic, colorectal, and lung cancers (3, 4).

KRAS is a small GTPase that cycles between inactive GDP-bound and active GTP-bound states, to transmit signals from cell surface receptors to regulate cellular processes (5). The intrinsic GTP hydrolysis and nucleotide exchange rates of KRAS are low, and the nucleotide cycle is controlled by additional regulators enabling KRAS activity to be carefully modulated (5). Guanine exchange factors (RASGEFs), such as SOS1 and SOS2, promote exchange of GDP for GTP to positively regulate KRAS activity (6). In contrast, GTPase-activating proteins (RASGAPs), such as p120GAP and NF1, stimulate GTP hydrolysis returning KRAS to an inactive GDP-bound form (7).

Two flexible regions within KRAS (switch-I and switch-II) are important for regulating protein–protein interactions forming distinct conformational states depending upon which nucleotide is bound, with GTP-KRAS able to bind and activate effector proteins (8). The best characterized KRAS effectors are RAFs, which regulate the RAF-MEK-ERK or MAPK signaling pathway, and the p110 catalytic subunits of Class IA PI3K which regulate the PI3K-AKT-mTOR pathway. Other RAS effector proteins have been also reported including RalGDS, Tiam1, and PLC-ε (9, 10).

Oncogenic KRAS mutation are predominantly found at glycine 12 (G12), glycine 13 (G13), or glutamine 61 (Q61), with G12 mutations accounting for the majority (3, 4). These mutations impair intrinsic and/or GAP-induced GTP hydrolysis (11) favoring the formation of GTP-bound active KRAS and driving aberrant activation of downstream signaling pathways to promote cancer cell survival and proliferation (12, 13). KRAS^{G12C} is an oncogenic mutant isoform with a glycine to cysteine alteration at codon 12 (c.34G>T). *KRAS*^{G12C} mutations are most prevalent in lung adenocarcinoma (∼12%) but are also found at a lower frequency in colon (∼3%) and pancreatic adenocarcinoma (∼1%) [The Cancer Genome Atlas (TCGA) PanCancer Atlas].

Until recently KRAS had been considered an intractable target, due to lack of druggable pockets and high-affinity nucleotide binding. However, the discovery of a novel binding pocket in the switch-II region of KRAS^{G12C} enabled development of the first irreversible targeted inhibitor of mutant KRAS, trapping it in an inactive GDP-bound state (14). Molecules with improved potency and pharmacologic properties have since been developed and demonstrated compelling antitumor activity in *KRAS*^{G12C} preclinical models (15–17). Sotorasib (AMG510) and adagrasib (MRTX849) were the first inhibitors to enter clinical trials and have reported favorable safety profiles with encouraging clinical benefit at least in some patients with advanced *KRAS*^{G12C} tumors (18–21). The data from the CodeBreaK100 trial (NCT03600883) have led to the FDA granting accelerated approval for sotorasib to treat patients with locally advanced or metastatic *KRAS*^{G12C} non–small cell lung cancer (NSCLC).

Here we report the characterization of AZD4625, a novel potent and selective irreversible inhibitor of oncogenic KRAS^{G12C}, in a range of preclinical studies. We demonstrate that AZD4625 binds and selectively inhibits KRAS^{G12C}, driving broad antitumor activity of *in vitro* and *in vivo KRAS*^{G12C} preclinical tumor models. Furthermore, we also report that combinations with other anticancer agents, including those that can improve the blockade of the RAS pathway and immunotherapy agents, can deepen and improve duration of response to AZD4625.

Materials and Methods

Materials and cell lines

AZD4625, SHP099, and afatinib were synthesized in-house as per published methods (22, 23). RMC-4550 was purchased from Selleckchem. Anti-mPD-L1 (mouse IgG1, clone D265A), anti-mPD-1 (mouse IgG2a, clone RMP1-14), and isotype controls were synthesized in-house. For *in vitro* studies, compounds were solubilized in

[1]AstraZeneca, Cambridge, United Kingdom. [2]AstraZeneca, Waltham, Massachusetts.

A. Chakraborty, L. Hanson, and D. Robinson contributed equally to this article.

Corresponding Author: Sarah Ross, Bioscience, Oncology R&D, AstraZeneca, Cambridge CB2 0RE, United Kingdom. Phone: +44 (0) 7584 909550; E-mail: sarah.ross@astrazeneca.com

Mol Cancer Ther 2022;21:1535–46

doi: 10.1158/1535-7163.MCT-22-0241

DMSO. For animal studies, AZD4625, afatinib, and RMC-4550 were formulated in 0.5% HPMC/0.1% Tween 80 (HPMC/Tween), SHP099 in 1% Pluronic and antibodies in PBS (phosphate-buffered saline).

Cells were routinely grown in RPMI or DMEM supplemented with 10% FCS and 2 mmol/L glutamine at 37°C in 5% CO_2. Cells were used in studies between passage 2 and 10. All cell lines were authenticated by short tandem repeat analysis upon banking and/or stock replenishment and periodically screened by PCR for *Mycoplasma* and rodent pathogens for *in vivo* studies. Details of cells including cancer type and source are in Supplementary Table S1.

Generation of CT26^{G12C} model

The *KRAS*^{G12C} mutation was introduced into CT26.WT (ATCC CRL-2638, RRID:CVCL_7256) by CRISPR/Cas9 technology (Supplementary Fig. S1A). A total of 0.5×10^6 CT26 cells were combined with ribonucleoprotein complex (22 pmol synthetic single-guide RNA (sgRNA) and 18 pmol recombinant Cas9) and 50 pmol of homologous directed repair template and electroporated using the Neon electroporation system 10 μL Kit (Thermo Fisher Scientific). Single-cell clones, produced by FACS (BD FACSJazz), were expanded and genomic DNA isolated by DirectPCR Lysis Reagent (Viagen). Mutation frequency was determined by digital droplet PCR using the QX200 System (Bio-Rad) and confirmed that clones P5E11 and P5E6 had biallelic G12C mutations (Supplementary Fig. S1B).

The sgRNA, HDR template, and primer and probe sequences are detailed in Supplementary Materials and Methods.

Cellular assays

Incucyte proliferation and apoptosis assay

NCI-H358 (ATCC CRL-5807, RRID:CVCL_1559) were seeded at 2,000 cells/well in 384-well plates (Greiner) in 40 μL of growth media. After 24 hours, cells were dosed with compounds and 1.5 μmol/L NucView 488 caspase 3/7 reagent (Sigma) using a HP liquid dispenser (Tecan) and imaged for 120 hours on an Incucyte (Sartorius). Images were analyzed using Incucyte software, apoptosis normalized units were derived by normalizing apoptotic nuclei number to cell confluence.

Five-day two-dimensional proliferation assay

Two-dimensional (2D) proliferation was assessed by seeding cells into 384-well plates (Greiner) in 70 μL of growth media at 250–1,000 cells/well. Plates were incubated for 24 hours and either processed immediately (day 0) or dosed with compounds using an Echo 555 liquid handler (Labcyte) and incubated for a further 5 days. The number of dead and live cells at days 0 and 5 were determined using a SYTOX green assay. In brief, 2 μmol/L SYTOX green nucleic acid dye (Thermo Fisher Scientific) was added (5 μL/well) and incubated for 1 hour at 37°C. The number of green cells (dead cells) was measured using an Acumen Explorer imager (TTP Labtech) using laser voltage at 425 V. Cells were then permeabilised overnight at room temperature with 10 μL/ well 0.25% (w/v) Saponin (Sigma) before recounting for a total cell count. Number of live cells were calculated by subtracting the dead cell count from the total cell count.

Proliferation of semiadherent, suspension, and cells growing in clumps were assessed by measuring ATP content using CellTiter-Glo (Promega). Cells were plated and dosed as described above. On days 0 or 5, 35 μL of CellTiter-Glo was added and incubated for 1 hour at room temperature. Luminescence was measured in a SpectraMax i3 reader (Molecular Devices).

Data were normalized to day 0 and analyzed using Genedata Screener (Genedata AG, RRID:SCR_022506).

Three-dimensional soft agar proliferation assay

For anchorage-independent growth, soft agar proliferation assays were performed. A total of 1,500–5,000 cells/well were seeded in 75 μL of 0.3% agar onto a 50 μL 1% agar layer in RPMI growth media. The agar layers were covered with 50 μL of growth media and compounds dosed using a HP D300 Digital Dispenser (Tecan) considering the combined agar/media compartments in the well. A total of 50 μL of fresh media and compound was added every 7 days. A GelCount (Oxford Optronix) was used to monitor the number of colonies above a threshold of 40 or 70 μm diameter, with the final reading when 150–400 colonies had formed in control wells (dependent on the cell line). Data were analyzed using GraphPad Prism 8 (RRID:SCR_002798).

Time to regrowth proliferation assay

Cells were seeded into 48-well plates (Corning) at 1×10^4 (NCI-H358) or 4×10^3 (NCI-H1373) cells/well in 500 μL growth media. The following day fresh media containing compound treatment was added and was replaced every 3–4 days. After 14 days, all compound treatments were stopped. Cell confluency was measured on an Incucyte ZOOM (Sartorius).

Cell-cycle analysis

A total of 1×10^6 NCI-H358 cells were seeded into 10 cm dishes (Nunc), incubated for 24 hours and then dosed with compound. At indicated timepoints, cells were detached with TripLE Express (Thermo Fisher Scientific), washed with PBS, and fixed with 70% EtOH for 1 hour on ice. Cells were washed in PBS and incubated in 1 mg/mL of RNase A (Sigma) in 0.5 mL PBS for 1 hour on ice. Propidium iodide (Invitrogen) at a final concentration of 50 μg/mL in 0.5 mL PBS was added, incubated for 15 minutes and cell cycle analyzed on a Fortessa flow cytometer (BD Biosciences).

Protein analysis of *in vitro* tumor lines

Protein extraction

For standard signaling and mass spectrometry target engagement assays, samples were prepared as follows. Cells were seeded into 6-well plates and after 24 hours dosed with compound and incubated for the indicated period. Cells were washed in ice-cold PBS and lysed in cell lysis buffer [137 mmol/L NaCl, 20 mmol/L TrisHCl, pH 7.4, 10% volume per volume (v/v) glycerol, 1% (v/v) Triton X-100, 0.5% weight per volume (w/v) sodium deoxycholate, 0.1% (w/v) SDS, 2.0 mmol/L EDTA; inhibitors of proteases and phosphatases (Merck) were added immediately prior to use]. Lysates were centrifuged and protein quantified in collected supernatants using a BCA kit (Thermo Fisher Scientific).

RAS activity

Cell seeding and dosing were carried out as described above. A total of 16 hours postdose, cells were washed in ice-cold PBS containing 2 mmol/L $MgCl_2$ and lysed using RAS Activity Buffer (Thermo Fisher Scientific). Cell lysates were centrifuged, supernatants collected, and protein quantified. GTP-bound active RAS was isolated from 100 mg total protein with the Active Ras Pull-Down and Detection Kit (Thermo Fisher Scientific) using 40 mg of GST-CRAF-RBD. Samples were analyzed by Western blotting.

Western blotting

Proteins were separated on 4%–12% Bis-Tris or 3%–8% Tris-Acetate NuPAGE gels in MOPs, MES or Tris-Acetate SDS running buffers and transferred onto nitrocellulose membrane using an iBlot Dry Blotting System (Thermo Fisher Scientific). Membranes were blocked for 1 hour in 5% milk or 5% BSA in TBST or PBST [TBS (Tris-

buffered saline) or PBS containing 0.05% Tween-20] and then incubated with primary antibody at 4°C overnight on a rocking platform. Membranes were washed 3× 15 minutes with TBST or PBST, incubated with horseradish peroxidase–conjugated secondary antibody, washed 3× 15 minutes with TBST or PBST and developed using SuperSignal West Dura or West Femto substrate (Thermo Fisher Scientific). Proteins were visualized on a G-BOX imager and quantified using the GeneTools software (Syngene, RRID:SCR_022505). The antibodies used are detailed in Supplementary Table S2.

Mass spectrometry target engagement

Samples for target engagement analysis were spiked with an equal protein concentration of lysate derived from cells grown in SILAC media containing $^{13}C_6$ lysine as a loading control. Ras protein was immunoprecipitated from the pooled extracts with an anti-Ras antibody (clone RAS10, Millipore, catalog no. 05-516, RRID: AB_2121151). Immunoprecipitated material was sequentially washed with RIPA buffer (Sigma), PBS and water. Protein was denatured with 10 mmol/L dithiothreitol in 50 mmol/L ammonium bicarbonate at 65°C for 20 minutes. Cysteine residues were alkylated with 50 mmol/L iodoacetamide for 30 minutes at room temperature. Trypsin was added at a final concentration of 0.1 μg/μL and samples incubated overnight at 37°C. The resulting peptides were dried by centrifugal evaporation and stored at –20°C until analysis.

Peptides were resuspended in 0.1% (v/v) formic acid and analyzed with an Acquity M-Class UPLC (Waters) coupled to a Xevo TQ-S triple quadrupole mass spectrometer (Waters). Peptide separation was achieved at a flow rate of 300 nL/minute across a 15 cm HSS T3 column (Waters) with a 20-minute gradient ranging from 5% to 40% acetonitrile, 0.1% formic acid. The Xevo TQS was operated in multiple reactions monitoring mode with the transitions described in Supplementary Table S3. Peak integration was performed in TargetLynx (Waters) and the ratio of endogenous: heavy calculated per peptide. The KRAS^{G12C} peptide area for each sample was normalized to the pan RAS peptide signal. Target engagement was calculated as a percentage relative to the vehicle control.

Animal studies

All experimental work conducted is detailed in an approved project license and has been reviewed by an internal Ethical Review Process. All work conducted in the UK adheres to the Animal Scientific Procedures Act 1986. All work involving the use of animals at, or on the behalf of, AstraZeneca complies with the company's Global Bioethics Policy.

In vivo studies were performed at either AstraZeneca [NCI-H358, NCI-H2122 (ATCC CRL-5985, RRID:CVCL_1531), LU99 (JCRB JCRB0080, RRID:CVCL_3015), CT26^{G12C} and *Kras^{G12C};Trp53$^{-/-}$* genetically engineered mouse model (GEMM)], Champions Oncology (CTG-1361, CTG-2011, CTG-2579, CTG-2539, CTG-2487, CTG-2536, CTG-0192, CTG-2751, CTG-2026, CTG-0147, CTG-1489, CTG-0387) or Crown Bioscience (CR1451, CR2528). Pathogen-free animals were housed in pathogen-free conditions under controlled conditions of temperature (19°C–23°C), humidity (55% ± 10%), photoperiod (12 hours light/12 hours dark), and air exchange. Animals were housed in individually vented cages, with food and water provided *ad libitum*.

AZD4625, afatinib, SHP099, and RMC-4550 were dosed orally in a volume of 0.1 mL/10 g. In combination studies, the combining oral agent was given 4 hours prior to AZD4625. Antibodies were administered by intraperitoneal injection and in combination immediately following the oral dose of AZD4625.

For subcutaneous efficacy studies, tumors were measured twice or thrice weekly by calliper and volume calculated using elliptical formula (pi/6 × width × width × length). Animal bodyweight and tumor condition were also recorded for the duration of the study. For the efficacy response, the %TGI (tumor growth inhibition) was assessed against the relative tumor volume at the end of the study. For pharmacokinetic-pharmacodynamic analysis, animals were humanely sacrificed at specified timepoints postdosing, tumor samples harvested, snap frozen in liquid nitrogen, and stored at −80°C before processing.

Xenograft studies

For NCI-H358, NCI-H2122, and LU99 xenograft studies, cells were prepared on the day of implant at a concentration of 3×10^6, 2.5×10^6, 5×10^6 cells, respectively, in a 50:50 ratio of matrigel:cells. A total of 0.1 mL cell suspension/mouse was subcutaneously implanted into the left flank of male athymic nude-Foxn1nu mice (Envigo UK, Strain ID: HSD-069). Once a mean tumor volume of approximately 0.2 cm^3 for efficacy studies or 0.5 cm^3 for pharmacokinetic-pharmacodynamic studies was reached, mice were randomized into relevant treatment groups. For CT26 (G12C clone P5E6) xenograft studies, 5×10^5 cells were implanted subcutaneously into the right flank of female BALB/cOla mice (Envigo UK, Strain ID: HSD-162). Mice were randomized into relevant treatment groups once a mean tumor volume of approximately 0.2 cm^3 was reached.

Patient-derived xenograft studies

For patient-derived xenograft (PDX) studies, female athymic nude-Foxn1nu mice (Envigo UK, Strain ID: HSD-069; Champions Oncology) or female BALB/cNj nude mice (GemPharmatec China, Stain ID: D000521; Crown Bioscience) were implanted on the left or right flank with relevant tumor tissue from stock animals. Once tumors reached an average tumor volume of 0.1–0.3 cm^3, mice were randomized into treatment groups.

Genetically engineered orthotopic lung tumor model

Lung tumors were induced in ODIn Cas9 mice (ODIn) as described previously (24). In summary, to induce Cas9 expression water with 2 mg/mL of doxycycline and 1% sucrose was provided for 3 days to 10-week-old C57Bl/6 ODIn mice. An adeno-associated virus bearing *Kras* and *Trp53* targeting sgRNAs was then administered (oropharyngeal route, 5×10^{10} GC/mouse). Treatment was started 11.5 weeks post-induction, when both adenomas and adenocarcinomas are present. For histologic analysis, lung tissue was inflated and fixed in 4% neutral buffered formalin. Paraffin sections were stained with hematoxylin and eosin (H&E) and tumor burden quantified using the HALO image analysis platform.

Gene profiling of *in vivo* tumor samples

RNA extraction

A total of 30 mg frozen tumor was homogenized in 650 μL of RLT buffer (Qiagen) for 2×3 minutes at 50 Hz in a TissueLyser LT (Qiagen). Following centrifugation RNA was extracted using the RNeasy Mini Kit on a QIACube following manufacturer's instructions (Qiagen). RNA concentration and quality were measured using a NanoDrop 2000 Spectrometer (Thermo Fisher Scientific).

Targeted qRT-PCR analysis

Gene expression was determined by qRT-PCR with 20 ng of RNA using the QuantiTect RT PCR Kit (Qiagen). Reactions were run in triplicate and performed on a LightCycler 480 (Roche) using the

following protocol: (i) 50°C 30 minutes, (ii) 95°C 15 minutes, (iii) 40 cycles of 95°C 15 seconds and 60°C 1 minute. On run completion, automatic thresholds were set, and C_t values generated. Gene expression was normalized to housekeeper and percent inhibition (or fold change) determined relative to vehicle. Statistically significant changes were determined using ANOVA analysis.

Fluidigm profiling and analysis

Reverse transcription was performed using 50 ng of RNA with a Reverse Transcription kit (Thermo Fisher Scientific) and cDNA was preamplified (14 cycles) using a pool of TaqMan primers, following the manufacturer's instructions (Fluidigm). Sample and assay preparation of the 96.96 Fluidigm Dynamic arrays were carried out according to the manufacturer's instructions. Data were collected and analyzed using Fluidigm Real-Time PCR Analysis 2.1.1 software (Fluidigm Real-time PCR Analysis software, RRID:SCR_015686) and C_t values used to calculate ddC_t and fold change. Significant *P* values were calculated by performing a Student *t* test on the -ddC_t values. Signature scores were calculated per sample as the mean of the expression of the genes (-dC_t) in each signature and *P* values calculated using a two-sample *t* test. Data was plotted using TIBCO Spotfire software (RRID:SCR_008858).

Primers and probes

Predesigned TaqMan FAM MGB primer and probe gene expression assays were from Thermo Fisher Scientific (Supplementary Table S4).

Protein profiling of *in vivo* tumor samples

Protein extraction

Frozen tumor pieces were lysed in ice-cold lysis buffer (as described in *in vitro* protein extractions) using a FastPrep-24 homogenizer (MP Biomedicals). In brief, samples were homogenized in 400 µL of buffer, sonicated for 30 seconds at high amplitude (Diagenode), then homogized again with an additional 400 µL of buffer. Samples were incubated on ice for 30 minutes before centrifuging and collecting supernatants. Protein concentrations were determined using a BCA assay kit (Thermo Fisher Scientific).

Western analysis

A total of 45 µg of total protein were used in Western analysis as described for *in vitro* studies.

Mass spectrometry target engagement

Target engagement measurement was essentially performed as described for *in vitro* samples except to enable quantification of samples from tumor extracts synthetic stable isotope coded peptides (Cambridge Research Biochemicals) were added prior to LC/MS analysis. Peak integration was performed in TargetLynx and the amount of free $KRAS^{G12C}$ calculated. Statistically significant changes in free $KRAS^{G12C}$ (unbound) from control samples were determined by ANOVA analysis.

Data availability statement

The data generated in this study are available within the article and its Supplementary data.

Results

AZD4625 binds and inhibits cellular $KRAS^{G12C}$

AZD4625 is a covalent allosteric inhibitor of $KRAS^{G12C}$ interacting with GDP bound-$KRAS^{G12C}$ to potently inhibit functional activity with an IC_{50} of 0.003 µmol/L (22).

Cellular potency and selectivity of AZD4625 was assessed in NCI-H358 cells, a human lung cancer model which carries a heterozygous $KRAS^{G12C}$ mutation. AZD4625 binds selectively to cellular $KRAS^{G12C}$ in NCI-H358 cells in a concentration dependent manner. Binding is dependent upon the cysteine-12 residue present in the mutant isoform with no interaction with wild-type RAS peptides observed (Supplementary Fig. S2A). Target engagement correlated with robust inhibition of the interaction between KRAS and the Ras-binding domain of CRAF, reduction in KRAS effector pathway signaling and modulation of cell-cycle arrest and apoptosis biomarkers (Supplementary Fig. S2B). Kinetic analysis demonstrated maximal cellular binding of AZD4625 to $KRAS^{G12C}$ by 3 hours of treatment with almost complete inhibition of MAPK pathway signaling (pCRAF, pMEK, pERK, p-RSK90) also being observed at this timepoint (**Fig. 1A** and **B**). In contrast, inhibition of PI3K pathway biomarkers (pAKT, pS6) and induction of apoptotic biomarkers (PDCD4, BIM, and cleaved PARP) were not observed until 16 hours of incubation of cells with compound (**Fig. 1B**). Consistent with $KRAS^{G12C}$ inhibition, AZD4625 reduced proliferation and survival of NCI-H358 cells driving cell-cycle arrest and apoptosis (**Fig. 1C** and **D**).

AZD4625 inhibited RAS signaling (Supplementary Fig. S3), and the proliferation of multiple $KRAS^{G12C}$ cancer cells across different tumor tissues in 2D cell growth assays (**Fig. 1E**). Target engagement and pathway inhibition was broadly similar across $KRAS^{G12C}$ cells although maximal and duration of response varied, likely due to multiple factors including availability of GDP-bound $KRAS^{G12C}$ (Supplementary Fig. S3). A range of AZD4625 antiproliferative activity was observed with 15 of 25 cells having a GI_{50} of less than 200 nmol/L and 4 of 25 cells having a GI_{50} of greater than 3 µmol/L (**Fig. 1E**; Supplementary Table S5). AZD4625 showed minimal antiproliferative activity in all the six non-$KRAS^{G12C}$ mutant and $KRAS^{WT}$ cancer cells in the 2D assay, with a GI_{50} of 2.5 µmol/L or greater (**Fig. 1E**; Supplementary Table S5). Anchorage-independent 3D proliferation of NCI-H358 and MIA PaCa-2 $KRAS^{G12C}$ cells were also robustly inhibited by AZD4625, with minimal impact on the growth of A549 ($KRAS^{G12S}$) or PC9 ($KRAS^{WT}$) cells in this assay format (**Fig. 1F**).

AZD4625 has a similar mechanism of action to sotorasib (AMG510) and adagrasib (MRTX849) and as expected shows comparable antiproliferative activity *in vitro* (Supplementary Fig. S4). Some differences in activity were noted, primarily in the extent of stasis and cytotoxity observed across both $KRAS^{G12C}$ and $KRAS^{WT}$ cells (Supplementary Fig. S4B), suggesting subtle differences in compound profile.

Taken together, these data confirm that the novel compound AZD4625 is a potent and selective inhibitor of cellular $KRAS^{G12C}$ with a similar profile to other $KRAS^{G12C}$ inhibitors.

AZD4625 inhibits the growth of $KRAS^{G12C}$ mutant tumors *in vivo*

AZD4625 has favorable pharmacokinetic properties with good oral bioavailability in mouse (22); therefore, target engagement and efficacy was explored *in vivo* in $KRAS^{G12C}$ lung cancer xenografts. Mass spectrometry analysis of NCI-H358 and NCI-H2122 tumors following a single oral treatment of tumor-bearing mice with AZD4625 at 100, 20, or 4 mg/kg demonstrated dose dependent binding of the compound to $KRAS^{G12C}$, that correlated with plasma exposure (**Fig. 2A** and **B**; Supplementary Tables S6 and S7; Supplementary Fig. S5A and S5B). MAPK pathway activity was also inhibited in tumors with expression of *DUSP6* and *FOSL1* mRNA transcripts being significantly reduced (**Fig. 2A** and **B**; Supplementary Tables S6 and S7). Western analysis of tumors further demonstrated KRAS inhibition by AZD4625 with reductions in MAPK (pMEK1/2, pERK1/2, p-p90RSK)

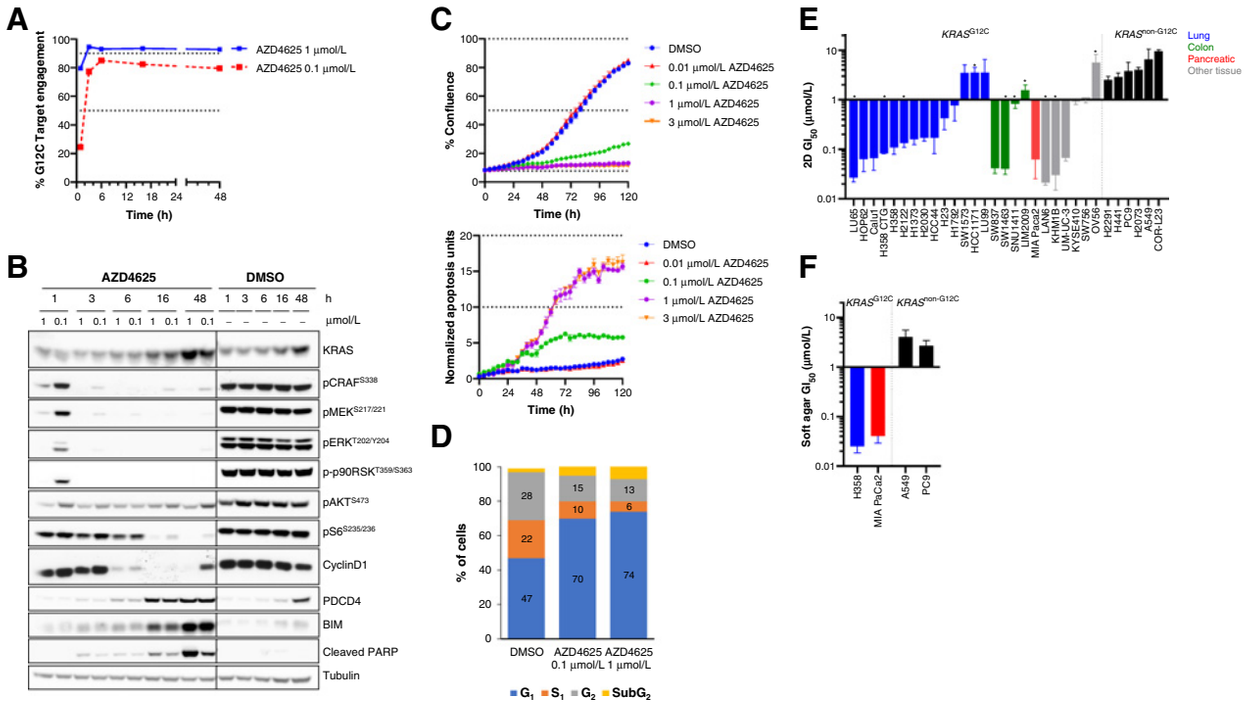

Figure 1.

AZD4625 selectively binds and inhibits cellular KRAS^{G12C}. **A** and **B,** Binding of AZD4625 to KRAS^{G12C} (% target engagement) measured by mass spectrometry and biomarker modulation in lysates from NCI-H358 cells dosed with 0.1 or 1 µmol/L of AZD4625. Samples were collected at 1, 3, 6, 16, and 48 hours postdosing. AZD4625- and DMSO-treated NCI-H358 cell lysates were analyzed in parallel. Line indicates physical separation on the Western blot analysis. **C,** Proliferation and apoptosis of NCI-H358 cells following treatment with a dose range of AZD4625. **D,** Cell-cycle profiling of NCI-H358 cells following treatment with 0.1 or 1 µmol/L of AZD4625 for 4 hours. **E,** Inhibition of cellular proliferation by AZD4625 in 2D assays. Data shown are the geometric mean of the GI_{50}, error bars represent geometric SD factor. Proliferation was measured after 5 days of compound treatment by either a nuclei count or CellTiter-Glo assay endpoints. Data generated using CellTiter-Glo are indicated by the asterisk. **F,** Inhibition of anchorage-independent cellular growth by AZD4625 in soft agar assays. Data shown represent the geometric mean, error bars represent geometric SD factor.

and PI3K (pAKT, pS6) pathway biomarkers (Supplementary Fig. S5C and S5D).

Chronic daily treatment of tumor-bearing mice with AZD4625 inhibited the growth of the *KRAS*^{G12C} xenografts *in vivo*, with a daily dose of 100 mg/kg significantly inhibiting the growth of both models. In the NCI-H358 model, robust and sustained regressions were observed at 100 mg/kg and significant tumor growth inhibition at the lower doses of 20 and 4 mg/kg (**Fig. 2C**; Supplementary Table S8). In contrast to the NCI-H358 model and *in vitro* sensitivity, the NCI-H2122 xenografts appeared relatively resistant to AZD4625 treatment demonstrating modest but statistically significant antitumor activity with 100 and 20 mg/kg chronic dosing (**Fig. 2D**; Supplementary Table S9). All doses of AZD4625 were well tolerated with no effects on animal body weight on chronic daily dosing (Supplementary Fig. S6). Analysis of tumor samples taken after chronic treatment of AZD4625 demonstrated continued inhibition of *DUSP6* and *FOSL1* expression (Supplementary Fig. S6; Supplementary Tables S8 and S9) indicating sustained target engagement and MAPK pathway inhibition.

Tumor growth inhibition and regression were also observed with AZD4625 treatment in additional *KRAS*^{G12C} cell line–derived xenograft (CDX) and PDX spanning disease lineage and genetic heterogeneity (**Fig. 3A**; Supplementary Table S10). Consistent with the *in vitro* data there was a range of responses, with the lung tumor models appearing broadly more sensitive to AZD4625 than colorectal. AZD4625 also showed strong antitumor activity in established *Kras*^{G12C};*Trp53*$^{-/-}$ lung tumors *in situ* generated in the ODIn (ObLiGaRe doxycycline-inducible) Cas9 mouse model (24). This model has tightly controlled doxycycline-inducible Cas9 expression and generates multifocal lung adenocarcinomas when sgRNA to modify *Kras* and *Trp53* are delivered to the lung following Cas9 expression induction (24). Treatment with AZD4625 led to a significant reduction in lung tumor burden in this GEMM within 7 days of treatment (**Fig. 3B** and **C**).

Combinations that inhibit receptor tyrosine kinase activity deepen and extend the duration of response to AZD4625

The activity of receptor tyrosine kinases (RTK) may modulate sensitivity to AZD4625. This could be through driving KRAS^{G12C} into a GTP-bound state, which would be insensitive to drug. Alternatively, RTKs may reduce KRAS^{G12C} dependency by activating cellular proliferation and survival pathways through wild-type RAS isoforms or alternative RAS-independent mechanisms (25, 26). Therefore, we explored the combination of AZD4625 with anticancer agents inhibiting RTK activity. In both NCI-H358 and NCI-H1373 lung models monotherapy treatment with 0.1 µmol/L of AZD4625 inhibited cellular proliferation; however, the depth and duration of response at this suboptimal dose of AZD4625 was improved when combined with inhibitors of EGFR (gefitinib), ErbB (afatinib), or SHP2 (SHP099; **Fig. 4A–C**). Biomarker analysis demonstrated increased

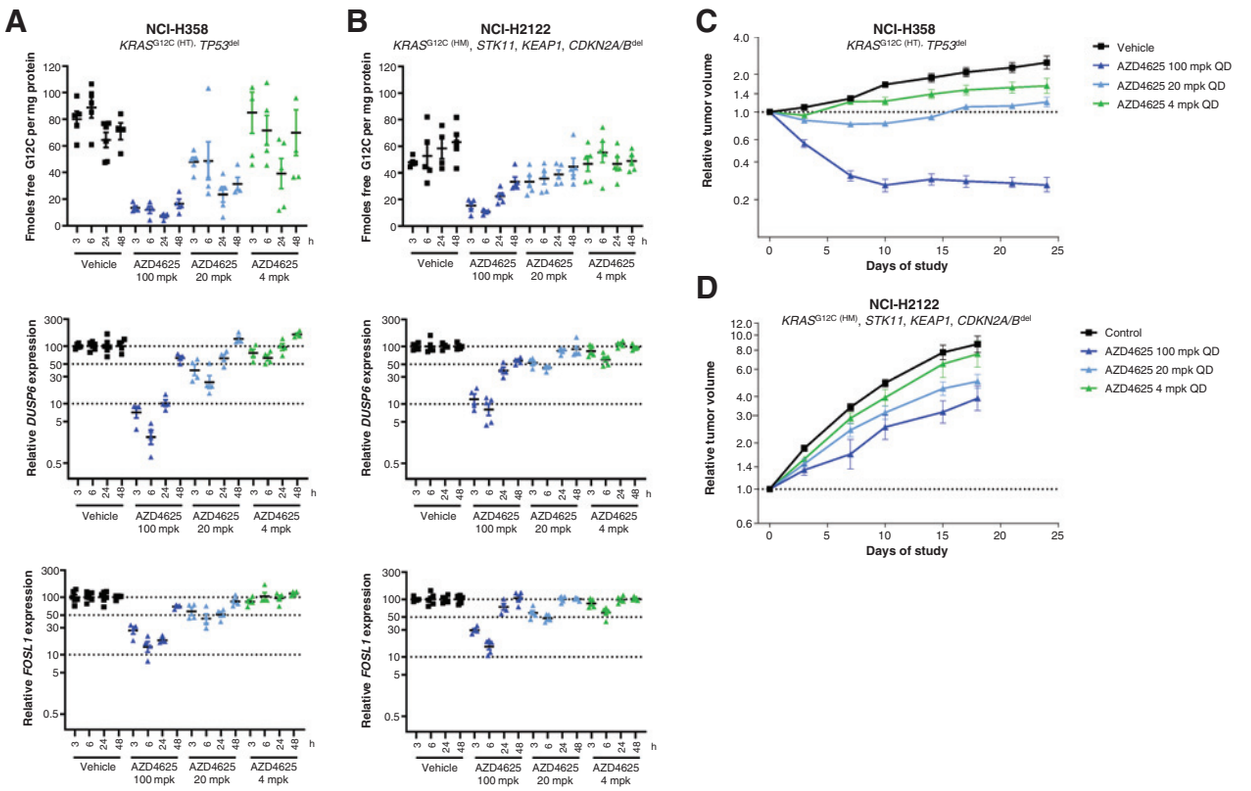

Figure 2.

AZD4625 inhibits the growth of *KRAS*^{G12C} mutant tumors *in vivo*. Target engagement of AZD4625 in NCI-H358 (**A**) or NCI-H2122 (**B**) tumors following a single oral treatment of mice with 100, 20, or 4 mg/kg of compound. Target engagement was measured by a reduction in free KRAS^{G12C} protein by mass spectrometry or by inhibition of *DUSP6* or *FOSL1* mRNA. *DUSP6* and *FOSL1* expression was normalized to *POLR2A* and relative to time matched vehicle controls. Data shown are individual animal, mean and SEM. Relative tumor volume of subcutaneous NCI-H358 (**C**) or NCI-H2122 (**D**) tumors with daily oral dosing of AZD4625. Data shown are geometric mean and error. Average start tumor volume was 0.28 cm^3 for NCI-H358 tumors and 0.193 cm^3 for NCI-H2122 tumors.

and extended duration of MAPK/PI3K pathway inhibition, as well as enhanced apoptosis with combination treatments (**Fig. 4D** and **E**). In addition, afatinib and SHP2 inhibitor combination with AZD4625 increased AZD4625 binding to KRAS^{G12C} (Supplementary Fig. S7).

These data indicated that AZD4625 combinations with inhibitors targeting multiple RTKs could be of particular benefit, with SHP099 driving sustained regressions and afatinib achieving superior combination activity compared with gefitinib in both models at clinically relevant doses. To explore further, afatinib and SHP2 inhibitor combinations with AZD4625 were assessed in NCI-H358 and LU99 lung xenograft models *in vivo*. Chronic treatment of mice with 100 mg/kg daily dose of AZD4625 drove significant antitumor activity in monotherapy in both of these xenografts (**Fig. 5A**–**D**; Supplementary Tables S11–S14). Therefore, to explore the potential combination benefit, AZD4625 was lowered to 20 mg/kg in NCI-H358 and 50 mg/kg in LU99.

In the NCI-H358 model, 20 mg/kg AZD4625 achieved 74% TGI in monotherapy increasing to 93% TGI in combination with a well-tolerated clinically relevant dose of afatinib (**Fig. 5A**; Supplementary Fig. S8; Supplementary Table S11). The SHP2 inhibitor combination achieved even greater responses with 55% tumor regression on codosing 20 mg/kg AZD4625 and 100 mg/kg SHP099 (**Fig. 5C**; Supplementary Table S13); however, this was accompanied with unexpected bodyweight loss (Supplementary Fig. S8). The LU99 model was less responsive to AZD4625 with 50 mg/kg monotherapy treatment driving 53 or 57% TGI (**Fig. 5B** and **D**; Supplementary Tables S12 and S14). Afatinib or SHP099 combinations with AZD4625 showed greater antitumor activity when compared with dose-matched monotherapy treatments. SHP099 combinations were particularly effective with 67% regressions being achieved with 50 mg/kg codosing. Importantly, the combination of AZD4625 with SHP099 at 50 mg/kg was well tolerated in the LU99 study with no bodyweight changes (Supplementary Fig. S8). The activity of the AZD4625 in combination with afatinib and SHP099 were also explored in *KRAS*^{G12C} lung and colorectal PDX models (**Fig. 5E** and **F**; Supplementary Fig. S9). Chronic treatment of mice with AZD4625 coadministered with afatinib or SHP099 generally enhanced antitumor activity when compared with dose-matched AZD4625 monotherapy treatment in lung PDX models; however, SHP099 combinations were more broadly active (6/6 models) and achieved deeper regressions than afatinib (**Fig. 5E** and **F**). The SHP099, but not the afatinib, combination was also able to drive increased antitumor activity compared with AZD4625 monotherapy in colorectal PDX models (Supplementary Fig. S9).

In the clinic, SHP2 inhibitors are being explored with intermittent dosing schedules (27). Therefore, to evaluate the potential clinical relevance of this combination, we compared efficacy with daily or intermittent codosing of SHP2 inhibitors (SHP099 or RMC-4550) with AZD4625 (**Fig. 5G** and **H**). SHP099 or RMC-4550, codosed daily or on a "2 days on 5 days off" weekly schedule with 100 mg/kg daily

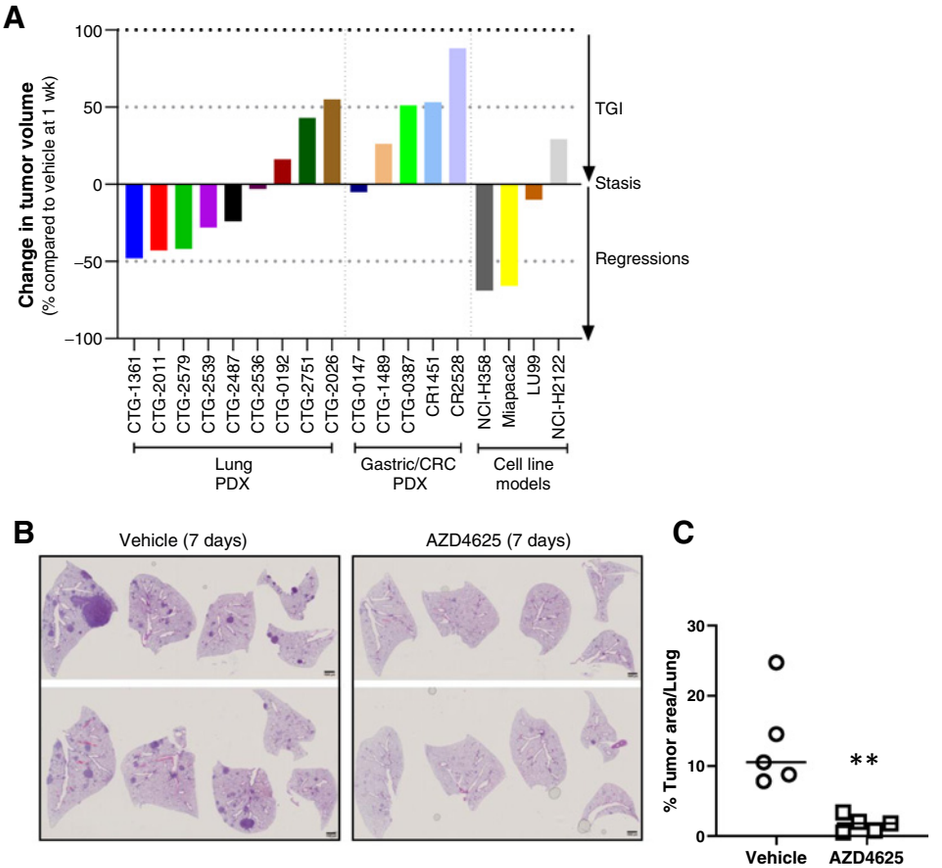

Figure 3.

AZD4625 inhibits the growth of *KRAS*^{G12C} mutant PDX models and murine lung *KRAS*^{G12C} tumors *in situ*. **A,** Antitumor activity of AZD4625 across a panel of *Kras*^{G12C} mutant *in vivo* models. Tumor-bearing mice were treated with daily oral dosing of AZD4625 at 100 mg/kg. Data shown are change in tumor volume compared with vehicle control following 1 week of continuous dosing. **B,** Representative H&E-stained lung sections of *Kras*^{G12C}/*Trp53*$^{-/-}$ lung tumors from ODIn mice treated with vehicle or AZD4625 for 7 days, once lung tumors were established (scale bar: 1,000 μmol/L). **C,** Relative lung tumor burden per lung section/mouse ($n = 5$ mice/treatment group). **, *P*: 0.0060 (*t test*).

dose AZD4625 achieved robust regression of LU99 tumors greater than monotherapy treatments (**Fig. 5G** and **H**; Supplementary Table S15). Importantly either lowering the daily dose or reducing dosing frequency of the SHP2 inhibitors had minimal impact on the combination benefit observed with AZD4625 as well as improving the tolerability of the combination (Supplementary Fig. S8).

Taken together, these data suggest that RTK inhibitor combinations could improve the monotherapy activity of AZD4625 and that inhibitors of multiple RTKs, such as SHP2 inhibitors, could be of particular benefit.

Immune checkpoint inhibitor combinations improve the response of a *KRAS*^{G12C} syngeneic mouse model

Oncogenic KRAS induces the expression of immune modulatory factors in tumors, which drives an immune suppressed tumor microenvironment (28). Therefore, KRAS^{G12C} inhibitors may augment the activity of immune checkpoint inhibitors (ICI) through generating a more favorable immune microenvironment (29). To explore potential combination opportunities for AZD4625 with ICIs, a CT26^{G12C} model was generated by CRISPR (Supplementary Fig. S1A and S1B). *In vitro* profiling confirmed the presence and functionality of the *Kras*^{G12C} allele with clone P5E6 being selected for *in vivo* work (Supplementary Fig. S1). AZD4625 activity alone or in combination with anti-PD-1 or anti-PD-L1 was then explored in the CT26^{G12C} model in immunocompetent mice (**Fig. 6**). The CT26^{G12C} model had a robust response to monotherapy AZD4625 at 100 mg/kg, with rapid tumor regressions and extended survival compared with vehicle control (**Fig. 6B**). However, even on continued AZD4625 treatment most tumors started to regrow and there were no complete responses. The addition of murine anti-PD-1 or anti-PD-L1 treatment with AZD4625 further improved responses, extending antitumor activity and driving some complete tumor regressions (**Fig. 6B**). There were four complete responders in combination with anti-PD-1 which were sustained beyond the cessation of dosing and two complete responders were observed in the anti-PD-L1 codosed group (**Fig. 6B**).

To confirm target engagement and explore changes in the immune cell composition and phenotype in CT26^{G12C} tumors following monotherapy and combination treatments, we utilized a targeted gene panel (Supplementary Table S4) and assessed modulation following 3 or 7 days of treatment (**Fig. 6C**). AZD4625 treatment at 100 mg/kg in monotherapy or combination reduced expression of *Dusp6* and *Fosl1* from 3 days consistent with target engagement and inhibition of KRAS^{G12C} activity (**Fig. 6D**). Modulation of the immune cell composition and microenvironment of the tumor was also evident on AZD4625 monotherapy and combination treatments (**Fig. 6E**; Supplementary Fig. S10).

Gene expression changes supportive of driving an antitumor immune response were observed with AZD4625 as a monotherapy or in combination with anti-PD-1/PD-L1. In addition to significant and sustained upregulation of transcripts associated with increased Cd8$^+$ T cells and Cd19$^+$ B cells (**Fig. 6E**; Supplementary Fig. S10A), there were increases in expression of genes linked with cytotoxic immune cell function (*Gzma*, *Nkg7*, and *Prf1*), antigen presentation (*B2m*, *H2K1*), dendritic cell maturation (*Batf3*) and increased expression of proinflammatory cytokines transcripts, such as *Ifng* and *Tnf* (Supplementary Fig. S10B and S10C). Genes encoding arginase (*Arg1*)

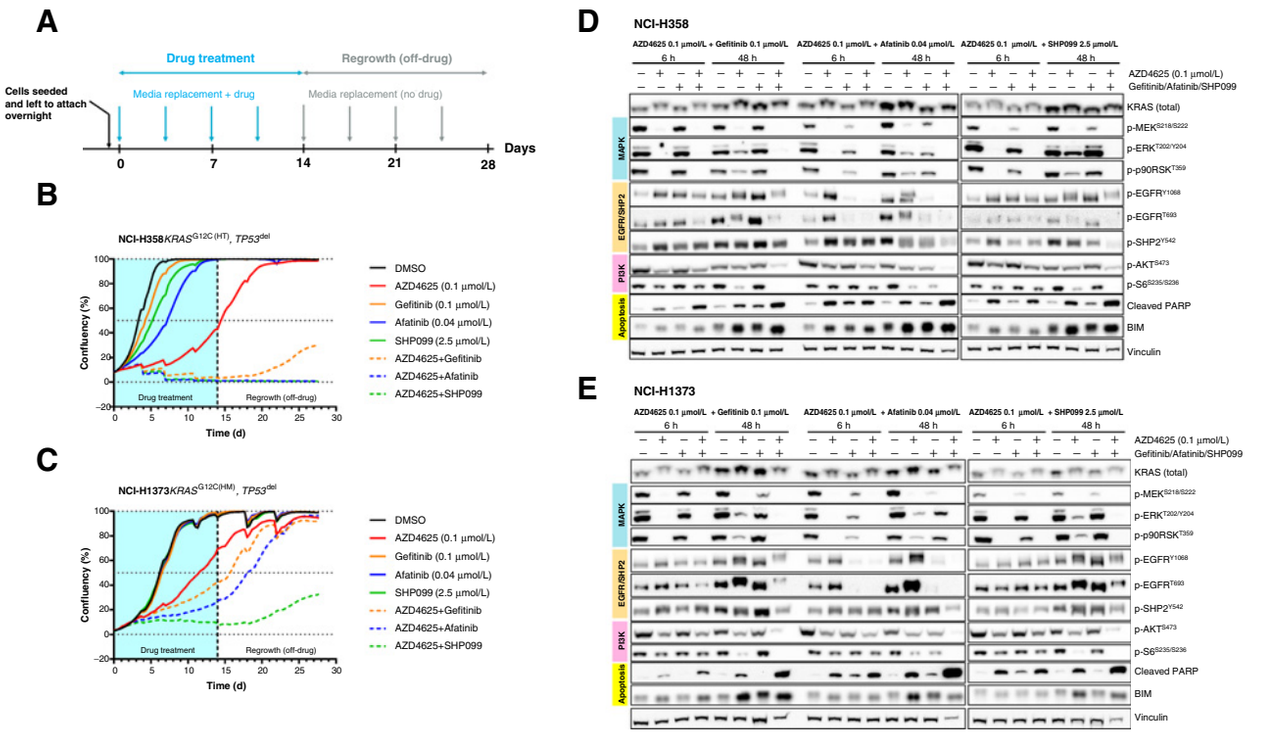

Figure 4.

RTK inhibitor combinations deepen and extend the duration of AZD4625 response *in vitro*. **A,** Schematic representation of dosing regimen used in proliferation assays. **B** and **C,** NCI-H358 or NCI-H1373 cells were treated with AZD4625, gefitinib, afatinib or SHP099 in monotherapy or in combination and cell growth continuously monitored as confluency using an imaging assay. After 14 days, compound treatments were removed, and regrowth of cells off-drug was assessed. Representative data from one of the independent assays are shown. The data plotted are the average from two wells. **D** and **E,** Western blot analysis of key biomarkers from NCI-H358 or NCI-H1373 cells following treatment with AZD4625 monotherapy or combinations.

and VEGF (*Vegfa*), involved in driving an immunosuppressive microenvironment, were also downregulated by AZD4625 monotherapy or combination treatments (Supplementary Fig. S10B). However, some gene expression changes within the tumor following treatment, including an increase in regulatory T cell (Treg) transcripts (*Foxp3*), increases in the expression of some checkpoint genes (*Ctla4*, *Lag3*, and *Pdcd1*) and induction of anti-inflammatory cytokines (*Il10*) could be more tumor promoting (Supplementary Fig. S10). All changes appeared to be predominantly driven by AZD4625 treatment.

Taken together, these data suggest AZD4625 can drive changes to the tumor immune microenvironment and that deeper and more durable responses may be achieved if AZD4625 is combined with ICIs.

Discussion

KRAS is frequently mutated or amplified in human tumors and effective targeted therapies for *KRAS* mutant cancers remain an unmet clinical need. The *KRAS*^{G12C} mutation is present in approximately 12% NSCLC (TCGA PanCancer Atlas) although differences in prevalence have been reported in Western (13%) and Asian (3.6%) populations (30). The *KRAS*^{G12C} mutation is also present in approximately 3% of colorectal cancer [TCGA PanCancer Atlas (30, 31)] and at lower frequencies in other solid tumors including pancreatic, endometrial, and bladder cancers [TCGA PanCancer Atlas (30)].

AZD4625 is a potent, selective and orally bioavailable KRAS^{G12C} inhibitor as demonstrated in biochemical and biophysical *in vitro* assays, in cellular assays and *in vivo* in preclinical models. *In vitro* and cellular assays have shown selective binding and inhibition of the KRAS^{G12C} isoform, which carries a glycine to cysteine mutation at residue 12, with no binding and inhibition of wild-type RAS or isoforms carrying other non-KRAS^{G12C} mutations.

Cellular studies confirmed that binding of AZD4625 to KRAS^{G12C} leads to inhibition of KRAS activity, inhibition of RAS regulated downstream signaling and induction of biomarkers of apoptosis. AZD4625 broadly inhibits *KRAS*^{G12C} cancer cell growth, with a range of potencies. Inhibition of proliferation is dependent upon the presence of the mutant cysteine-12 residue supporting a wide therapeutic margin. *In vivo* studies in *KRAS*^{G12C} xenografts have shown that orally dosed AZD4625 can bind to KRAS^{G12C} and inhibit downstream effector pathway activity in a dose-dependent manner. Chronic daily dosing of AZD4625 is well tolerated in preclinical models and can drive robust and sustained antitumor activity against *KRAS*^{G12C} tumors including PDX and primary lung tumors in GEMMs.

Although demonstrating broad activity, AZD4625 had a range of *in vitro* and *in vivo* antitumor responses, ranging from robust regression to relatively modest effects. This differential activity is not unexpected and has been reported for other KRAS^{G12C} inhibitors. Indeed, despite encouraging clinical data with sotorasib and adagrasib, especially in NSCLC, not all patients with *KRAS*^{G12C} mutant tumors respond robustly to treatment with a reported objective response rate to sotorasib of 37.1% in NSCLC (19) and a modest 9.7% in colorectal cancer (32). Reported rates of response to adagrasib are broadly similar (20). Differences in *KRAS*^{G12C} tumor response may reflect magnitude of target engagement, heterogeneity of the depth, and

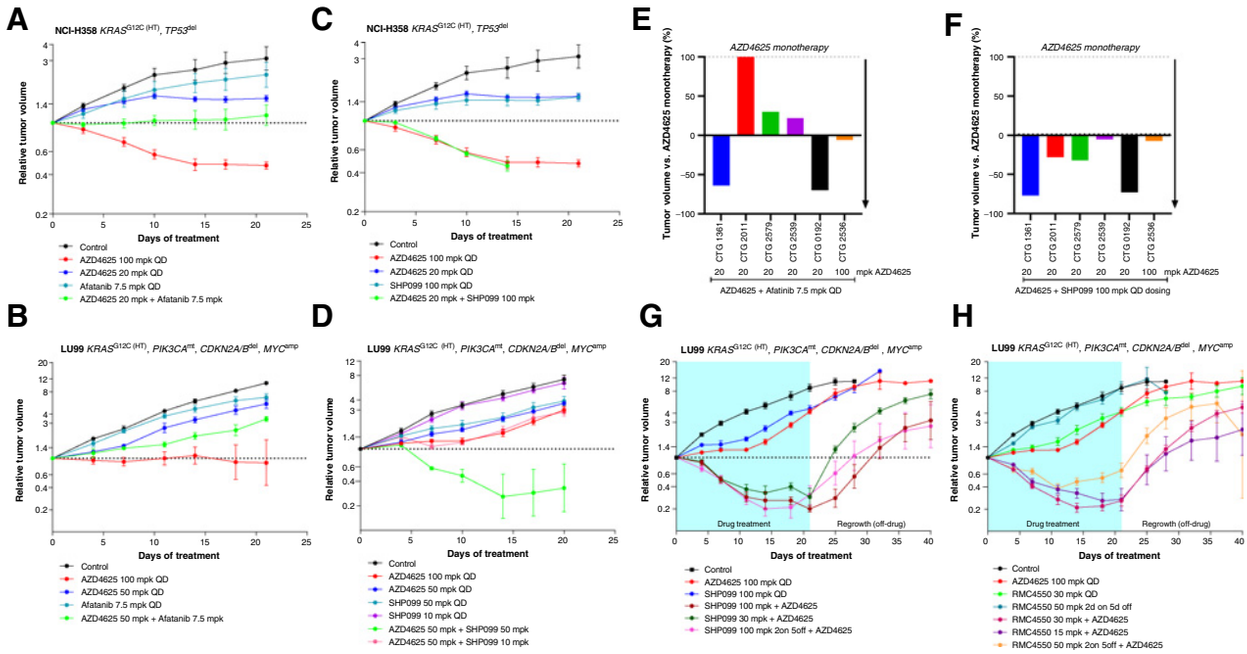

Figure 5.

RTK inhibitor combinations deepen and extend the duration of AZD4625 response *in vivo.* **A–D,** Relative tumor volume of subcutaneous NCI-H358 or LU99 tumors with daily oral dosing of mice with the indicated AZD4625, afatinib and/or SHP099 treatments. Average starting tumor volumes were 0.213 cm^3 for NCI-H358 tumors and either 0.304 cm^3 (**B**) or 0.398 cm^3 (**D**) for LU99 tumors. Data shown are geometric mean and error. AZD4625 in combination with 100 mg/kg daily dose of SHP099 (**C**) caused body weight losses and dosing was stopped on day 14. **E** and **F,** Change in tumor volume with afatinib or SHP099 combinations compared with dose-matched AZD4625 monotherapy across a panel of *KRAS*^{G12C} lung PDX models at end of dosing period. In these studies, mice with actively growing tumors were randomized into two groups and treated with vehicle or 100 mg/kg AZD4625 for 7 days to determine monotherapy response. Mice in the AZD4625 group were then rerandomized and treated with 100 or 20 mg/kg AZD4625 alone or in combination with afatinib or SHP099 at the doses indicated for 3 weeks. **G** and **H,** Relative tumor volumes of LU99 tumors with oral dosing of mice with 100 mg/kg daily dosing of AZD4625 and the indicated doses of SHP099 or RMC-4550. Average start tumor volume was 0.297 cm^3. Treatments were stopped at 3 weeks and tumor regrowth monitored. Data shown are geometric mean and error. SHP099 at 100 mg/kg dose on a continuous schedule in monotherapy or combination groups had some impact on bodyweight. Dosing was paused if individual animal bodyweight dropped below −15% and reintroduced when bodyweight recovered to −8%. Dosing of SHP099 was also stopped on days 16 + 17 for all animals in the 100 mg/kg continually dosing groups.

duration of effector pathway inhibition and intrinsic dependency on KRAS^{G12C}, likely impacted by co-occurring genetic alterations. Indeed, exploratory tumor biomarker analysis of NSCLC patients being treated with sotorasib suggests a potential lower response rate in patients with *KEAP1* comutated tumors compared with those with wild-type *KEAP1* (19). In addition, emerging data indicate acquired resistance mechanisms are likely to limit the duration of response with a median progression-free survival for sotorasib of 6.8 months in NSCLC (19). Potential clinical resistance mechanisms are beginning to emerge and appear diverse with both genetic and histological potential mechanisms of escape reported (33–35). Therefore, combination approaches are considered necessary to drive deeper and more durable patient responses. Furthermore, the mutant selective properties of KRAS^{G12C} inhibitors, which will limit normal tissue toxicities, are expected to enable tolerated dosing with additional therapeutic agents.

RTK activity may modulate sensitivity to KRAS^{G12C} inhibitors, such as AZD4625, through several mechanisms. First, AZD4625 selectively binds KRAS^{G12C} in its inactive GDP-bound confirmation, and RTK activity may drive it into a drug insensitive GTP-bound form through activation of SOS-mediated nucleotide exchange (36). Second, RTK activity may reduce dependency of the cancer cell on KRAS^{G12C} through activating proliferation and survival pathways through wild-type RAS isoforms or through RAS-independent mechanisms (25, 26). In addition, as MAPK pathway activity phosphorylates and negatively regulates upstream activators of RAS, including RTKs, such as EGFR and FGFR (37), KRAS^{G12C} inhibitor treatment is likely to lead to enhanced RTK activity therefore driving adaptive feedback. The importance of EGFR signaling in *KRAS*^{G12C} colorectal cancer is emerging from the clinic, with monoclonal EGFR antibody combinations improving response rates of adagrasib and sotorasib (32, 38). We explored the combination treatments of AZD4625 with inhibitors of RTK activity including afatinib and SHP2 inhibitors. Afatinib is a second-generation ErbB family inhibitor which irreversibly binds and inhibits EGFR (ErbB1), HER2 (ErbB2), and HER4 (ErbB4; refs. 39, 40) and is approved for treating patients with metastatic NSCLC harboring specific EGFR mutations (41, 42). SHP2, encoded by the *PTPN11* gene, is a nonreceptor protein tyrosine phosphatase which is required for full activation of the RAS/MAPK signaling pathway downstream of RTKs through dephosphorylation of tyrosine residues in adaptor and scaffold proteins (43). The position of SHP2 as a common node downstream of multiple RTKs makes it an attractive target for combination with AZD4625. SHP099 and RMC-4550 are allosteric inhibitors of SHP2, which stabilize the protein in an autoinhibited conformation and are suitable for preclinical studies (44, 45).

Cellular and *in vivo* studies demonstrated the potential of afatinib and SHP2 inhibitor combinations to improve the therapeutic response of *KRAS*^{G12C} tumors to AZD4625 and this appeared to be through increased and extended target engagement and downstream RAS

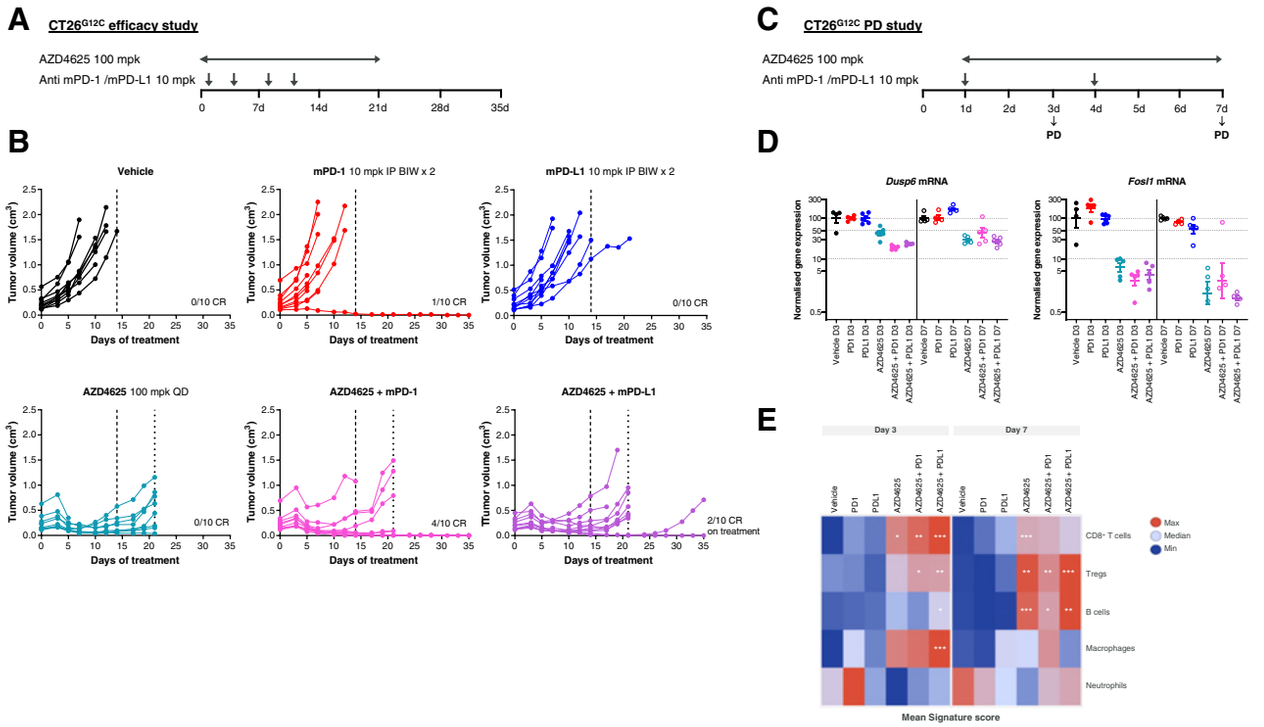

Figure 6.

Impact of AZD4625, anti-mPD-1, and anti-mPD-L1 monotherapy and combination treatments on CT26^{G12C} syngeneic tumors. **A,** Schematic of dosing for efficacy study. **B,** Tumor volumes of subcutaneous CT26^{G12C} tumors grown in immunocompetent Balb/c mice treated with AZD4625, anti-mPD-1, and anti-mPD-L1 in monotherapy or in combination. Dosing started 18 days post-implant when average tumor volume was 0.24 cm^3. Dashed line indicate day when all vehicle treated animals were off study. Dotted line indicates end of AZD4625 dosing. Animals showing a complete response at the end of the dosing period were monitored for tumor regrowth. Number of complete responders are indicated. **C,** Schematic of dosing and sample collection for pharmacodynamic study. Dosing started 15 days post-implant when average tumor volume was 0.36 cm^3. Samples were collected 6 hours after final dose of AZD4625. **D,** AZD4625 target engagement was measured by inhibition of *Dusp6* and *Fosl1* mRNA. Expression was normalized to averaged expression of housekeeper transcripts and relative to time-matched vehicle controls. Data shown are individual animal, mean, and SEM. **E,** Mean gene signature scores for indicated immune cell populations following 3 or 7 days of treatment. Data plotted are average score, scaled per signature. Asterisks indicate significant changes in score compared with time-matched control in the absence of AZD4625 with a *P* value of <0.05 (*), <0.01 (**), <0.001 (***).

pathway inhibition. SHP2 inhibitor combinations appeared to be more broadly active in both lung and colorectal models and drive greater combination responses likely by impacting signaling downstream of multiple RTKs. Indeed in the two *KRAS*^{G12C} colorectal PDXs, in contrast to SHP099, afatinib codosing showed no efficacy benefit, suggesting RTKs other than the ErbB family are limiting AZD4625 activity in these models. Interestingly, we did observe combination activity with cetuximab in the same models which could be through activation of natural killer cells and induction of antibody-dependent cellular cytotoxicity. Importantly, for SHP2 inhibitors, we have demonstrated that combination activity can be achieved with tolerated and clinically relevant intermittent dosing schedules.

ICIs have been found to be more efficacious and better tolerated than first-line platinum-based chemotherapy in NSCLC with high PD-L1 expression and some reports show patients with a *KRAS* mutation treated with ICIs derived better survival benefit than those treated with chemotherapy (46, 47). In addition, KRAS signaling has been reported to drive an immune suppressed tumor microenvironment (28) which is modulated on KRAS^{G12C} inhibition (29). Therefore, we explored the potential combination benefit of AZD4625 with ICIs. In a syngeneic CT26 *Kras*^{G12C} model AZD4625 initially drove robust tumor regressions; however even on continued treatment regrowth was observed. Codosing with antibodies blocking murine PD-1 or PD-L1 improved the rate and duration of antitumor response, particularly anti-PD-1, which achieved complete responses in 4 of 10 animals even after treatments were stopped. The increased antitumor response of combining AZD4625 with anti-PD-1 is in agreement with the result reported before with AMG510 (17) and MRTX849 (48). In addition, our data show that anti-PD-L1 in combination with AZD4625 also have increased efficacy, albeit lower than anti-PD-1.

Consistent with the reported role of oncogenic KRAS signaling in cross-talk with the tumor microenvironment (49) and the impact reported with other KRAS^{G12C} inhibitors (16, 48), AZD4625 treatment of the CT26^{G12C} model modulated gene expression signatures indicative of major changes in tumor immune cell population, phenotype, and microenvironment. The transcriptional changes with AZD4625 are complex and dynamic with both antitumor and protumor modulations observed. These changes were predominantly driven by AZD4625 treatment with little augmentation with anti-PD-1/PD-L1 combination therapies. Interestingly, on acute AZD4625 treatment when tumors are regressing, genes associated with cytotoxic T cells are expressed, however on chronic dosing when response is plateauing gene signatures associated with Tregs increase. Further understanding of how KRAS^{G12C} inhibition impacts both the tumor, and the tumor

immune microenvironment could help establish the mechanisms driving the combination activity observed with ICIs as well as identifying other potential combination partners.

In conclusion, the nonclinical pharmacology of AZD4625 shows that it has the potential to provide therapeutic benefit to patients with *KRAS*^{G12C} mutant cancer as either a monotherapy treatment or in combination with other targeted drug agents.

Authors' Disclosures

A. Chakraborty is an employee and shareholder of AstraZeneca. R. Whiteley is an AstraZeneca employee and shareholder. L. Magiera reports other support from AstraZeneca outside the submitted work. C.P. Martins is an AstraZeneca employee and shareholder. E. Wigmore reports personal fees from AstraZeneca outside the submitted work. Z. Underwood is an employee and shareholder of AstraZeneca. M. Niedbala reports personal fees from AstraZeneca during the conduct of the study. S.J. Ross is AstraZeneca employee and shareholder. No disclosures were reported by the other authors.

Authors' Contributions

A. Chakraborty: Investigation, visualization, methodology, writing–review and editing. **L. Hanson:** Investigation, visualization, methodology. **D.M. Robinson:** Investigation, visualization, methodology, writing–review and editing. **H. Lewis:** Investigation, visualization, methodology. **S. Bickerton:** Investigation, visualization, methodology. **M. Davies:** Conceptualization. **R. Polanski:** Investigation, visualization, methodology. **R. Whiteley:** Investigation, methodology. **A. Koers:** Supervision. **J. Atkinson:** Investigation, methodology. **T. Baker:** Investigation, methodology. **I. del Barco Barrantes:** Investigation, visualization, methodology. **G. Ciotta:** Resources, methodology. **J.G. Kettle:** Conceptualization. **L. Magiera:** Investigation, visualization, methodology. **C.P. Martins:** Supervision, writing–review and editing. **A. Peter:** Investigation, visualization, methodology. **E.M. Wigmore:** Visualization. **Z. Underwood:** Investigation, visualization, methodology. **S. Cosulich:** Conceptualization. **M. Niedbala:** Conceptualization. **S. Ross:** Conceptualization, supervision, writing–original draft.

Acknowledgments

We thank Michelle Porritt, Marcello Maresca, Mohammad Bohlooly, Simon Barry, Elizabeth Hardaker, and Lotte Martoft for support with GEMM development, and all the Oncology Bioscience team for support of studies and helpful discussions.

The costs of publication of this article were defrayed in part by the payment of page charges. This article must therefore be hereby marked *advertisement* in accordance with 18 U.S.C. Section 1734 solely to indicate this fact.

Note

Supplementary data for this article are available at Molecular Cancer Therapeutics Online (http://mct.aacrjournals.org/).

Received April 5, 2022; revised June 19, 2022; accepted August 3, 2022; published first August 5, 2022.

References

1. Sanchez-Vega F, Mina M, Armenia J, Chatila WK, Luna A, La KC, et al. Oncogenic signaling pathways in The Cancer Genome Atlas. Cell 2018;173:321–37.
2. Zehir A, Benayed R, Shah RH, Syed A, Middha S, Kim HR, et al. Mutational landscape of metastatic cancer revealed from prospective clinical sequencing of 10,000 patients. Nat Med 2017;23:703–13.
3. Cook JH, Melloni GEM, Gulhan DC, Park PJ., Haigis KM. The origins and genetic interactions of KRAS mutations are allele- and tissue-specific. Nat Commun 2021;12:1808.
4. Prior IA, Hood FE, Hartley JL. The frequency of Ras mutations in cancer. Cancer Res 2020;80:2969–74.
5. Moore AR, Rosenberg SC, McCormick F, Malek S. RAS-targeted therapies: is the undruggable drugged? Nat Rev Drug Discov 2020;19:533–52.
6. Buday L, Downward J. Many faces of Ras activation. Biochim Biophys Acta 2008;1786:178–87.
7. Bos JL, Rehmann H, Wittinghofer A. GEFs and GAPs: critical elements in the control of small G proteins. Cell 2007;129:865–77.
8. Pantsar T. The current understanding of KRAS protein structure and dynamics. Comput Struct Biotechnol J 2020;18:189–98.
9. Cox AD, Fesik SW, Kimmelman AC, Luo J, Der CJ. Drugging the undruggable RAS: Mission possible? Nat Rev Drug Discov 2014;13:828–51.
10. Chakraborty A, Linnane E, Ross S. Ras proteins as therapeutic targets. Biochem Soc Trans 2018;46:1303–11.
11. Hunter JC, Manandhar A, Carrasco MA, Gurbani D, Gondi S, Westover KD. Biochemical and structural analysis of common cancer-associated KRAS mutations. Mol Cancer Res 2015;13:1325–35.
12. Zafra MP, Parsons MJ, Kim J, Alonso-Curbelo D, Goswami S, Schatoff EM, et al. An *in vivo* KRAS allelic series reveals distinct phenotypes of common oncogenic variants. Cancer Discov 2020;10:1654–71.
13. Ricciuti B, Son J, Okoro JJ, Mira A, Patrucco E, Eum Y, et al. Comparative analysis and isoform-specific therapeutic vulnerabilities of KRAS mutations in non-small cell lung cancer. Clin Cancer Res 2022;28:1640–50.
14. Ostrem JM, Peters U, Sos ML, Wells JA, Shokat KM. K-Ras(G12C) inhibitors allosterically control GTP affinity and effector interactions. Nature 2013;503:548–51.
15. Janes MR, Zhang J, Li LS, Hansen R, Peters U, Guo X, et al. Targeting KRAS mutant cancers with a covalent G12C-specific inhibitor. Cell 2018;172:578–89.
16. Canon J, Rex K, Saiki AY, Mohr C, Cooke K, Bagal D, et al. The clinical KRAS (G12C) inhibitor AMG 510 drives anti-tumour immunity. Nature 2019;575:217–23.
17. Hallin J, Engstrom LD, Hargis L, Calinisan A, Aranda R, Briere DM, et al. The KRAS(G12C) inhibitor MRTX849 provides insight toward therapeutic susceptibility of KRAS-mutant cancers in mouse models and patients. Cancer Discov 2020;10:54–71.
18. Hong DS, Fakih MG, Strickler JH, Desai J, Durm GA, Shapiro GI, et al. KRAS (G12C) inhibition with sotorasib in advanced solid tumors. N Engl J Med 2020;383:1207–17.
19. Skoulidis F, Li BT, Dy GK, Price TJ, Falchook GS, Wolf J, et al. Sotorasib for lung cancers with KRAS p.G12C mutation. N Engl J Med 2021;384:2371–81.
20. Ou S-HI, Janne PA, Leal TA, Rybkin II, Sabari JK, Barve MA, et al. First-in-human phase I/IB dose-finding study of adagrasib (MRTX849) in patients with advanced KRAS(G12C) solid tumors (KRYSTAL-1). J Clin Oncol 40: 23s, 2022 (suppl; abstr 2530–8).
21. Janne PA, Riely GJ, Gadgeel SM, Heist RS, Ou SI, Pacheco JM, et al. Adagrasib in non-small-cell lung cancer harboring a KRAS(G12C) mutation. N Engl J Med 2022;387:120–31.
22. Kettle JG, Bagal SK, Bickerton S, Bodnarchuk MS, Boyd S, Breed J, et al. Discovery of AZD4625, a covalent allosteric inhibitor of the mutant GTPase KRAS(G12C). J Med Chem 2022;65:6940–52.
23. Garcia Fortanet J, Chen CH, Chen YN, Chen Z, Deng Z, Firestone B, et al. Allosteric inhibition of SHP2: identification of a potent, selective, and orally efficacious phosphatase inhibitor. J Med Chem 2016;59:7773–82.
24. Lundin A, Porritt MJ, Jaiswal H, Seeliger F, Johansson C, Bidar AW, et al. Development of an ObLiGaRe doxycycline inducible Cas9 system for preclinical cancer drug discovery. Nat Commun 2020;11:4903.
25. Hata AN, Shaw AT. Resistance looms for KRAS(G12C) inhibitors. Nat Med 2020;26:169–70.
26. Kim D, Xue JY, Lito P. Targeting KRAS(G12C): from inhibitory mechanism to modulation of antitumor effects in patients. Cell 2020;183:850–9.
27. Bendell J, Ulahannan S, Koczywas M, Brahmer J, Capasso A, Eckhardt SG, et al. 5 Oral - Intermittent dosing of RMC-4630, a potent, selective inhibitor of SHP2, combined with the MEK inhibitor cobimetinib, in a phase 1b/2 clinical trial for advanced solid tumors with activating mutations of RAS signaling. Eur J Cancer 2020;138:S8–S9.
28. Cullis J, Das S, Bar-Sagi D. Kras and tumor immunity: friend or foe? Cold Spring Harb Perspect Med 2018;8:a031849.
29. van Maldegem F, Downward J. Mutant KRAS at the heart of tumor immune evasion. Immunity 2020;52:14–6.
30. Nassar AH, Adib E, Kwiatkowski DJ. Distribution of KRAS (G12C) somatic mutations across race, sex, and cancer type. N Engl J Med 2021;384:185–7.

31. Yaeger R, Chatila WK, Lipsyc MD, Hechtman JF, Cercek A, Sanchez-Vega F, et al. Clinical sequencing defines the genomic landscape of metastatic colorectal cancer. Cancer Cell 2018;33:125–36.
32. Fakih M, Falchook GS, Hong DS, Yaeger RD, Chan E, Mather O, et al. 434P CodeBreaK 101 subprotocol H: Phase Ib study evaluating combination of sotorasib (Soto), a KRASG12C inhibitor, and panitumumab (PMab), an EGFR inhibitor, in advanced KRAS p.G12C-mutated colorectal cancer (CRC). Ann Oncol 2021;32:S551.
33. Awad MM, Liu S, Rybkin II, Arbour KC, Dilly J, Zhu VW, et al. Acquired resistance to KRAS(G12C) inhibition in cancer. N Engl J Med 2021;384: 2382–93.
34. Tanaka N, Lin JJ, Li C, Ryan MB, Zhang J, Kiedrowski LA, et al. Clinical acquired resistance to KRAS(G12C) inhibition through a novel KRAS switch-II pocket mutation and polyclonal alterations converging on RAS-MAPK reactivation. Cancer Discov 2021;11:1913–22.
35. Zhao Y, Murciano-Goroff YR, Xue JY, Ang A, Lucas J, Mai TT, et al. Diverse alterations associated with resistance to KRAS(G12C) inhibition. Nature 2021; 599:679–83.
36. Lito P, Solomon M, Li LS, Hansen R, Rosen N. Allele-specific inhibitors inactivate mutant KRAS G12C by a trapping mechanism. Science 2016;351: 604–8.
37. Caunt CJ, Sale MJ, Smith PD, Cook SJ. MEK1 and MEK2 inhibitors and cancer therapy: the long and winding road. Nat Rev Cancer 2015;15: 577–92.
38. Weiss J, Yaeger RD, Johnson ML, Spira A, Klempner SJ, Barve MA, et al. LBA6 KRYSTAL-1: Adagrasib (MRTX849) as monotherapy or combined with cetuximab (Cetux) in patients (Pts) with colorectal cancer (CRC) harboring a KRASG12C mutation. Ann Oncol 2021;32:S1294.
39. Li D, Ambrogio L, Shimamura T, Kubo S, Takahashi M, Chirieac LR, et al. BIBW2992, an irreversible EGFR/HER2 inhibitor highly effective in preclinical lung cancer models. Oncogene 2008;27:4702–11.
40. Solca F, Dahl G, Zoephel A, Bader G, Sanderson M, Klein C, et al. Target binding properties and cellular activity of afatinib (BIBW 2992), an irreversible ErbB family blocker. J Pharmacol Exp Ther 2012;343:342–50.
41. Sequist LV, Yang JC, Yamamoto N, O'Byrne K, Hirsh V, Mok T, et al. Phase III study of afatinib or cisplatin plus pemetrexed in patients with metastatic lung adenocarcinoma with EGFR mutations. J Clin Oncol 2013;31:3327–34.
42. Wu YL, Zhou C, Hu CP, Feng J, Lu S, Huang Y, et al. Afatinib versus cisplatin plus gemcitabine for first-line treatment of Asian patients with advanced non-small-cell lung cancer harbouring EGFR mutations (LUX-Lung 6): an open-label, randomised phase 3 trial. Lancet Oncol 2014;15:213–22.
43. Yuan X, Bu H, Zhou J, Yang CY, Zhang H. Recent advances of SHP2 inhibitors in cancer therapy: current development and clinical application. J Med Chem 2020; 63:11368–96.
44. Chen YN, LaMarche MJ, Chan HM, Fekkes P, Garcia-Fortanet J, Acker MG, et al. Allosteric inhibition of SHP2 phosphatase inhibits cancers driven by receptor tyrosine kinases. Nature 2016;535:148–52.
45. Nichols RJ, Haderk F, Stahlhut C, Schulze CJ, Hemmati G, Wildes D, et al. RAS nucleotide cycling underlies the SHP2 phosphatase dependence of mutant BRAF-, NF1- and RAS-driven cancers. Nat Cell Biol 2018;20:1064–73.
46. Borghaei H, Paz-Ares L, Horn L, Spigel DR, Steins M, Ready NE, et al. Nivolumab versus docetaxel in advanced nonsquamous non-small-cell lung cancer. N Engl J Med 2015;373:1627–39.
47. Kim JH, Kim HS, Kim BJ. Prognostic value of smoking status in non-small-cell lung cancer patients treated with immune checkpoint inhibitors: a meta-analysis. Oncotarget 2017;8:93149–55.
48. Briere DM, Li S, Calinisan A, Sudhakar N, Aranda R, Hargis L, et al. The KRAS (G12C) inhibitor MRTX849 reconditions the tumor immune microenvironment and sensitizes tumors to checkpoint inhibitor therapy. Mol Cancer Ther 2021;20:975–85.
49. Hamarsheh S, Gross O, Brummer T, Zeiser R. Immune modulatory effects of oncogenic KRAS in cancer. Nat Commun 2020;11:5439.